Research Article

Lang Shui* and Jianhui Fu

An investigation on as-cast microstructure and homogenization of nickel base superalloy René 65

https://doi.org/10.1515/htmp-2022-0245
received May 31, 2022; accepted September 12, 2022

Abstract: Nickel base superalloy René 65 is a cast-wrought derivative of René 88DT. Lower cost and comparable physical properties allow René 65 to serve as a promising candidate material for turbine disks in next-generation aeroengines. The cast-wrought route leads to significant segregation of solute elements during solidification of René 65, which should be reduced by a proper homogenization scheme. We use René 65 samples from a Ø 450 mm electros-slag remelting ingot (sample Disk I) and a Ø 250 mm pilot vacuum arc remelting ingot (sample Disk II) to investigate as-cast microstructure and homogenization schemes of the alloy. It is discovered that γ–γ′ eutectic phase, borides–carbides, and TiN are the major precipitated phases in as-cast René 65 and Ti, Nb, Mo, and W are the critically segregated elements. The temperature too high to homogenize René 65 is found to be ≥1,190°C due to defect generation and straightening grain boundaries, whereas 1,140°C is too low due to undissolving γ–γ′ eutectic phase. The acceptable temperature among the selected temperatures is found to be 1,160°C. Thermal compression using homogenized samples reveals that in Disk II 1,160°C for 50 h provides the lowest flow stress. Estimation based on kinetics predicts that the equivalent deformation effect in Disk I is obtained at 1,160°C for 82 h.

Keywords: wrought superalloy, homogenization, microstructure, segregation characteristics

*** Corresponding author: Lang Shui,** Department of Special Steel Technology, Chengdu Institute of Advanced Metallic Material Technology and Industry Co. Ltd., Chengdu, 610305, Sichuan, China; State Key Laboratory of Metal Material for Marine Equipment and Application, Anshan, 114009, Liaoning, China, e-mail: ustb1234@126.com
Jianhui Fu: Department of Special Steel Technology, Chengdu Institute of Advanced Metallic Material Technology and Industry Co. Ltd., Chengdu, 610305, Sichuan, China; State Key Laboratory of Metal Material for Marine Equipment and Application, Anshan, 114009, Liaoning, China

1 Introduction

Wrought superalloys have been used in turbine disk applications since 1950s. Nowadays, Inconel 718 is the superalloy, which is mostly used for turbine disks worldwide, whereas its working temperature is below 650°C, which is unsatisfactory for aeroengines of higher thrust–weight ratios. To address this issue, ATI Specialty Materials and General Electric Aviation from the USA developed alloy René 88DT through the powder metallurgy route, which is able to work as turbine disks above 650°C for prolonged service [1–7]. As powder metallurgy is involved, the cost of René 88DT is considerably high. To reduce the cost while retaining physical properties, René 65, a cast-wrought derivative of René 88DT, was developed [8–16]. The composition of René 65 is based on René 88DT as shown in Table 1, and its production employs traditional cast-wrought flowsheet that significantly reduces cost. In the literature, René 65 has been reported to exhibit satisfactory physical properties above 650°C, allowing it to serve as the material of key components in next-generation aeroengines [17–23]. Although the composition of René 65 is derived from René 88DT, the cast-wrought route leads to different microstructures and far more serious microsegregation than powder metallurgy due to redistribution of solute elements in solidification. In addition, a cast ingot is usually larger in size than products obtained via powder metallurgy, which makes microsegregation an even more serious problem to be concerned. In the cast-wrought route, homogenization of cast ingots prior to billet conversion is almost the only way to reduce segregation. At elevated temperatures, the diffusion of an element is governed by many factors, such as diffusivity of the element, the level of matrix distortion, concentration of other solute elements, etc. [24–28]. Hence, a suitable combination of temperature and time needed for solute elements to be homogeneous is subject to the change of alloy composition. That is to say, a suitable homogenization scheme for a certain

Table 1: Nominal composition of René 65 (%) [8–16]

C	Cr	Ni	Co	Fe	Ti	Al	Nb	Mo	W
0.03	16.0	Bal.	13.0	1.0	3.7	2.1	0.7	4.0	4.0

superalloy should be discussed, respectively. Moreover, homogenization is an energy costing process as the heating furnace is maintained at a temperature as high as 1,000°C or above for a relatively long duration. Homogenization may also bring some detrimental changes to microstructure, such as pores or coarse grains. As a result, to establish a proper homogenization scheme for René 65 in which reductions of segregation, energy cost, and side effect are comprehensively considered becomes a necessary task. The present study aims to discover a proper scheme for René 65 by lab-scale experiments with the aforementioned issues comprehensively considered.

2 Experimental methodology

In this article, we collected samples from two sources to conduct homogenization experiment. The first source is a René 65 disk of Ø 450 mm cut from the top end of an ingot that has undergone VIM (vacuum induction melting) and ESR (electros-slag remelting), and the other is a René 65 disk of Ø 250 mm cut from the top end of an ingot that has undergone 200 kg pilot VIM and VAR (vacuum arc remelting). In the present study, we name them Disk I and Disk II, respectively. The composition of these two sample disks is measured by direct reading spectrometry as shown in Table 2, where the composition of Disk I is measured at multiple locations and shown in ranges due to its larger size. The reason to select two different sample disks is that secondary dendritic arm space is an important factor in solute element diffusion, and it varies with the size of the ingot. Secondary dendritic arm space is usually determined by the rate of solidification. Generally, a smaller VAR or ESR ingot solidifies faster than a larger one due to a shorter distance from the core to the cooling wall of crucible, which results in a shorter mean secondary dendritic arm space in a smaller ingot than in a larger ingot. A greater mean secondary dendritic arm space indicates that it takes a longer time for a certain element diffusing to be homogeneous. Samples from two ingots of different sizes are able to demonstrate the impact of secondary interdendritic arm space on homogenization.

Samples for different homogenization schemes were blocks cut along radius of the sample disks as shown in Figure 1. In each run of homogenization, a sample block was put into the heating furnace when the preset homogenization temperature was reached, and then was taken out for air cooling as long as the preset duration was reached. Homogenization temperatures include 1,140, 1,160, 1,190, 1,220, and 1,240°C, and durations include 5, 10, 20, 25, 30, 40, 50, 70, and 80 h. The sample block was then machined into 15 mm × 15 mm × 15 mm metallographic specimens, which were subsequentially processed by rotary sand paper and polishing cloth, and etched by $CuSO_4$ + HCl + C_2H_5OH aqueous solution for metallographic observation. Samples for differential scanning calorimetry (DSC) analysis were Φ 3 mm × 1 mm tiny disks cut from the sample disk, where the DSC temperature rising rate was set to be 10 K·min^{-1}. Samples for Gleeble thermal compression were Φ 10 mm × 15 mm columns machined from the sample blocks that have undergone different homogenization schemes.

3 Results and discussions

3.1 As-cast microstructure analysis

3.1.1 Optical microscope (OM) morphology and secondary dendrite arm space (SDAS) measurement

Figure 2 shows OM of as-cast microstructure at the center, half radius, and the brink of the two René 65 sample disks. By measurement under OM, SDAS at each location is plotted in Figure 2. Each presented dot represents the average of ten measurements and the error bar denotes standard deviation of such ten measurements. In Disk I,

Table 2: Composition of René 65 sample disks (%)

	Al	Co	Cr	Mo	Nb	Ti	W	Fe	Ni
Disk I	2.19–2.20	13.40–13.49	16.17–16.27	4.10–4.18	0.695–0.752	3.53–3.69	3.61–3.68	0.21–0.22	55.73–56.12
Disk II	2.04	12.93	16.09	4.06	0.735	3.5	4.12	0.47	55.63

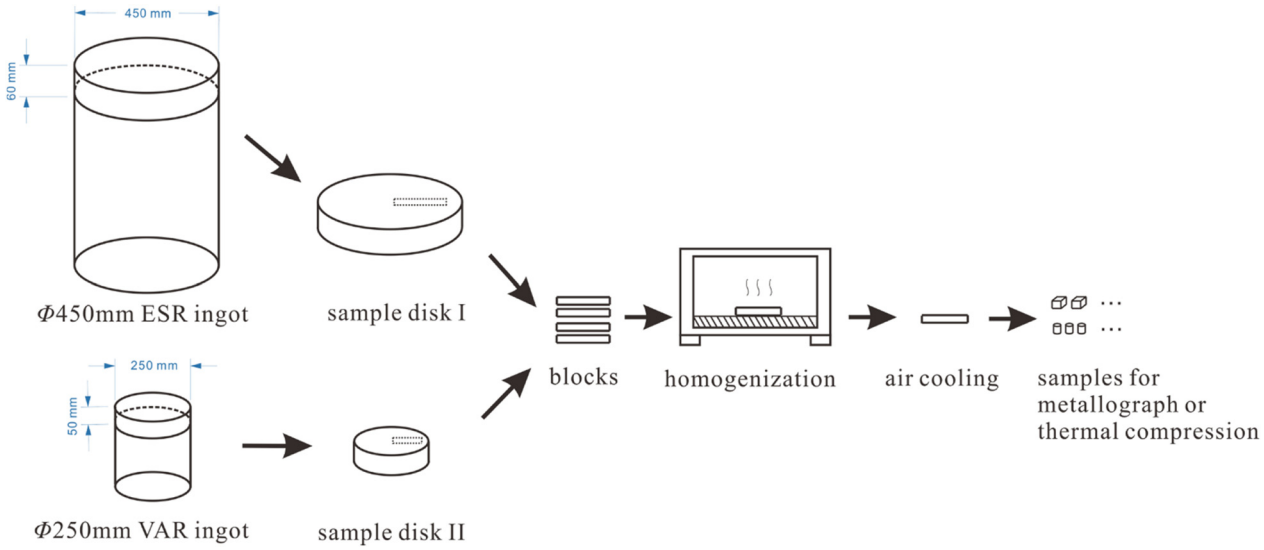

Figure 1: Schematic diagram of preparation procedure of samples.

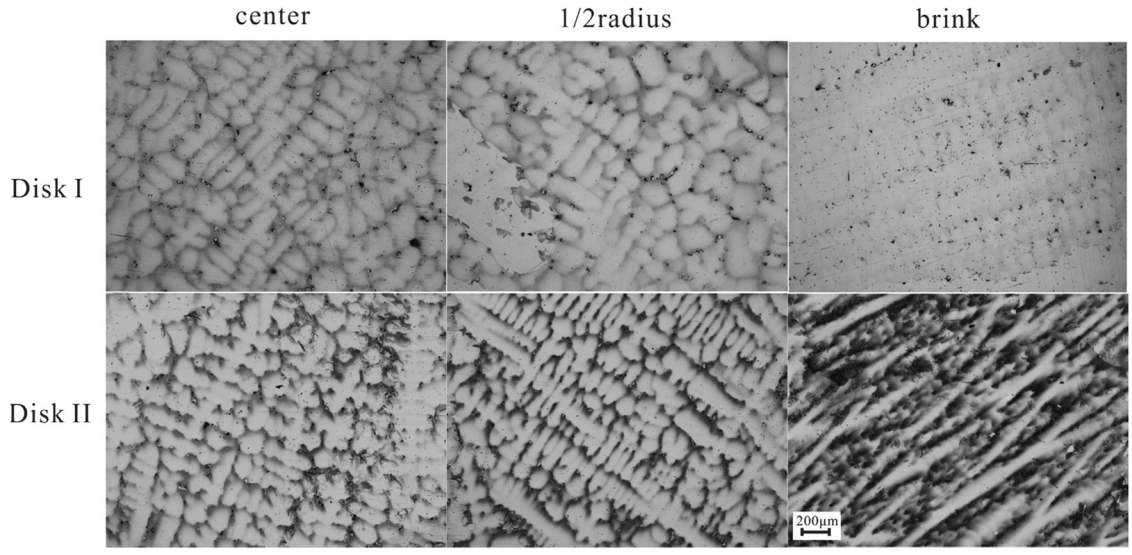

Figure 2: Morphology of as-cast microstructure under OM.

the SDAS at 1/2 radius is about 115 μm, which is the largest among the three sampling locations. In addition, the standard deviation (error bar) of ten measurements at 1/2 radius is the greatest as well, indicating that variation in SDAS at 1/2 radius is also in a great level. This is probably associated with complex solidification conditions at 1/2 radius of molten bath in the ESR crystallizer, which drives secondary dendrite arms to grow into a variety of distances. On the contrary, in Disk II, the average SDAS of each location is comparatively lower, only about 90 μm. Generally, SDAS is highly relevant to solidification rate. A smaller ingot usually is better cooled at the center and 1/2 radius than a larger one, hence it is easier for a smaller ingot to obtain a smaller SDAS. SDAS is a key factor for atom diffusion in matrix during homogenization [24,26,27]. A greater SDAS means a longer distance for atoms of a given element diffusing to be homogeneous. Therefore, for representativeness of the entire ingot, it is reasonable to use samples taken from the location with the greatest SDAS for the homogenization experiment (Figure 3).

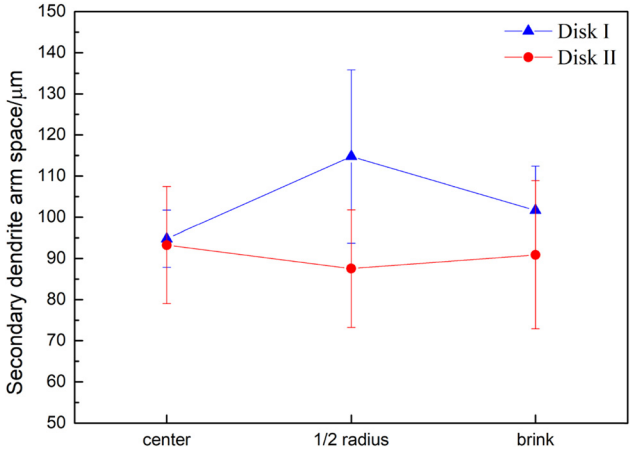

Figure 3: SDAS comparison between Disk I and Disk II.

3.1.2 Interdendritic phases and segregation coefficient of elements

Figure 4(a) is a computed phase diagram of René 65 at equilibrium. As shown in the diagram, initial melting temperature of René 65 is around 1,250°C, hence homogenization temperature of the alloy should not exceed this temperature. Figure 4(a) illustrates that γ′ phase is the major precipitated phase in this alloy, accounting for the greatest percentage other than γ matrix. σ phase and μ phase are topologically close-packed phases and usually precipitate in long-duration aging. Interstitial phases such as borides and carbides exist in a very small amount.

Figure 4(b) shows a scanning electron microscope (SEM) image of interdendritic regions of as-cast René 65. Three phases can be identified by energy-dispersive spectrometer (EDS), including γ–γ′ eutectic phase with γ′ phase arranged in fan-shapes at the edge, irregular borides–carbides that are closely adjacent to γ–γ′ eutectic phase, and scarcely dispersed polygonal TiN. γ′ phase, which is the major strengthening phase of René 65, disperses as tiny particles both dendritically and inter-dendritically. When γ–γ′ eutectic phase is formed at interdendritic regions during solidification, γ′ phase forms far-smaller particles in γ–γ′ eutectic phase than in dendritic regions, as shown in Figure 4(b). Due to γ′ phase dispersion hardening, γ–γ′ eutectic phase becomes harder and more brittle than matrix, which consequentially leads to cracking along eutectic blocks during subsequential deformation. Therefore, in order to obtain better ductility, γ–γ′ eutectic phase should be dissolved in homogenization prior to forge. Borides–carbides and TiN are reported not detrimental to alloy physical properties as long as they are in a small amount and exist sparsely in matrix, hence they are not specially considered in homogenization [8,9,29–32]. As a result, γ–γ′ eutectic phase is the key phase that needs to be dissolved in homogenization of as-cast René 65.

Figure 5 illustrates the DSC curve of René 65, where it shows that there is no notable peak under the initial melting temperature, indicating that there is no phase transition other than eutectic phase dissolving during temperature elevation. The DSC curve also shows that the initial melting point of René 65 is about 1,250°C, which is consistent with the computed phase diagram.

The origin of segregation during solidification of alloys is redistribution of solute elements. Generally, segregation coefficient K is used to characterize the extent of segregation for engineering purposes. For a given element, the definition of segregation coefficient K is expressed as: K = interdendritic mass percentage/dendritic mass percentage. According to this definition, the value of K approaching to unity indicates that the extent

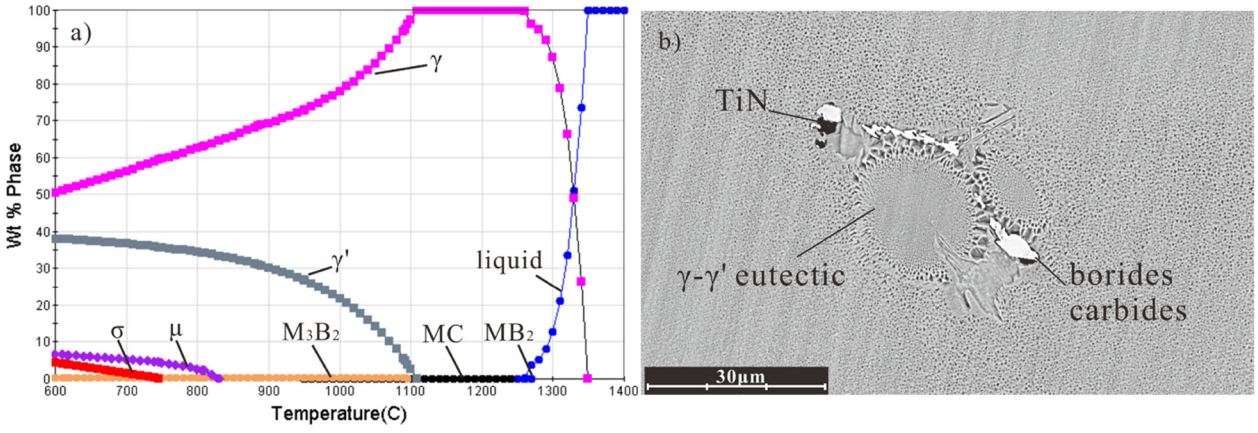

Figure 4: (a) Phase diagram of René 65 at equilibrium and (b) typical interdendritic phases in as-cast René 65.

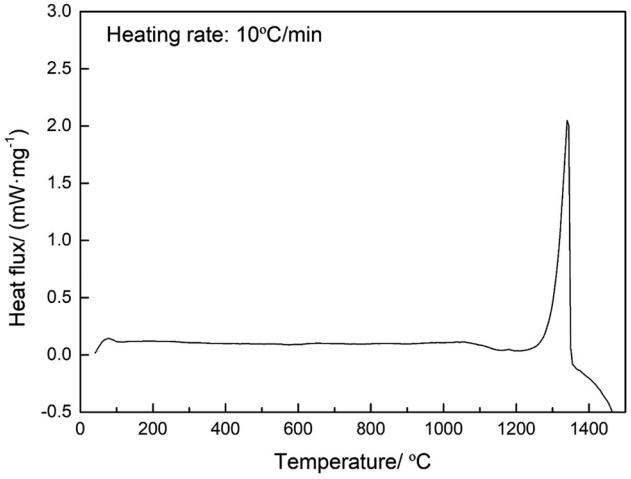

Figure 5: DSC heating curve of as-cast René 65.

of segregation is low. $K > 1$ indicates that the element tends to concentrate at interdendritic regions, and $K < 1$ indicates that the element tends to concentrate at dendrites. The present study employs SEM and EDS to measure segregation of element, and the procedure is as follows. At 700 times magnification, 10 points are probed at dendrites and interdendritic regions, respectively. The ratio of mean value of the ten points at interdendritic regions to that of dendrites is considered as measured K value of the sample. Measurement is conducted on samples taken from the center, 1/2 radius and brink of the aforementioned sample disks, and the results are shown in Figure 6. As it is illustrated, segregation level of Ti, Nb, W, and Mo is relatively high among those elements in the alloy, where Ti, Nb, and Mo concentrate at interdendritic regions while W concentrates at dendrites. In both Disks I and II, segregation of Ti, Nb, Mo, and W at the center and 1/2 radius is more critical than that at brink. Such a difference in the segregation level is relevant to slower solidification at the center and 1/2 radius compared to that at the brink because slower solidification provides enough redistribution time for the solute elements. Therefore, samples covering the region of disk center and 1/2 radius for homogenization are more representative in respect of homogenization. Each sample used for homogenization in the present study contains these regions of the sample disks, as shown in Figure 1.

3.2 Homogenization results

3.2.1 Microstructure evolution in homogenization

In order to discover a proper homogenization scheme, mitigation of segregation, dissolving of detrimental phases, and growth of grains should be comprehensively considered. As a cast-wrought superalloy, homogenization of René 65 can be optimized on the basis of Inconel 718. Common homogenization temperatures of Inconel 718 include 1,160 and 1,190°C. Considering René 65 is alloyed with elements of greater atom radii such as W and Mo, we add schemes of higher temperatures, 1,220 and 1,240°C, for the comparison of microstructure evolution of René 65 at a variety of conditions.

Figure 7 shows evolution of microstructure of samples from Disk I under SEM. It is shown that homogenizing at 1,160°C for 10 h has dissolved γ–γ′ eutectic phase of as-cast René 65 while grain boundaries are still clearly visible. In addition, one may still distinguish the profile of dendrites by black–white contrast in the image,

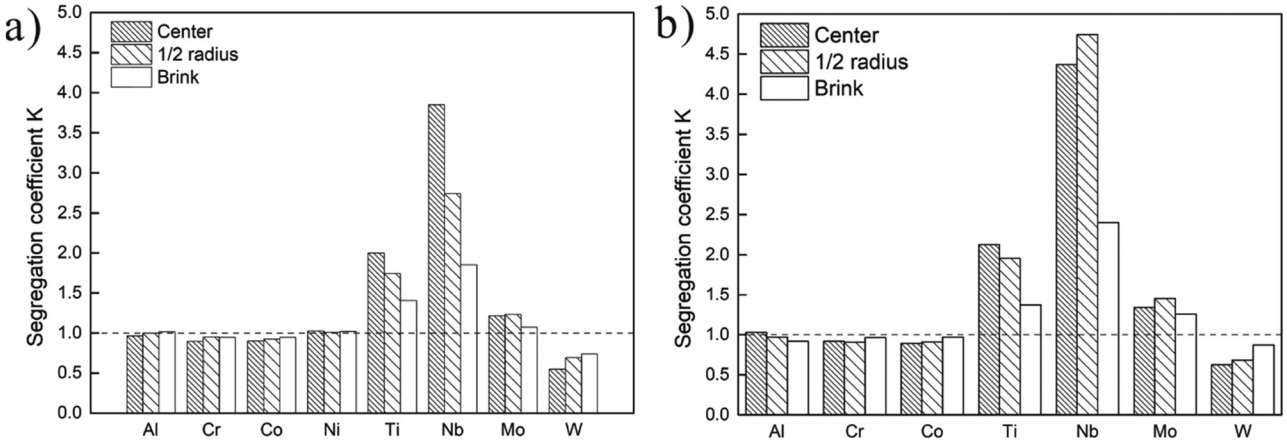

Figure 6: Segregation coefficient K of elements in as-cast René 65: (a) sample Disk I and (b) sample Disk II.

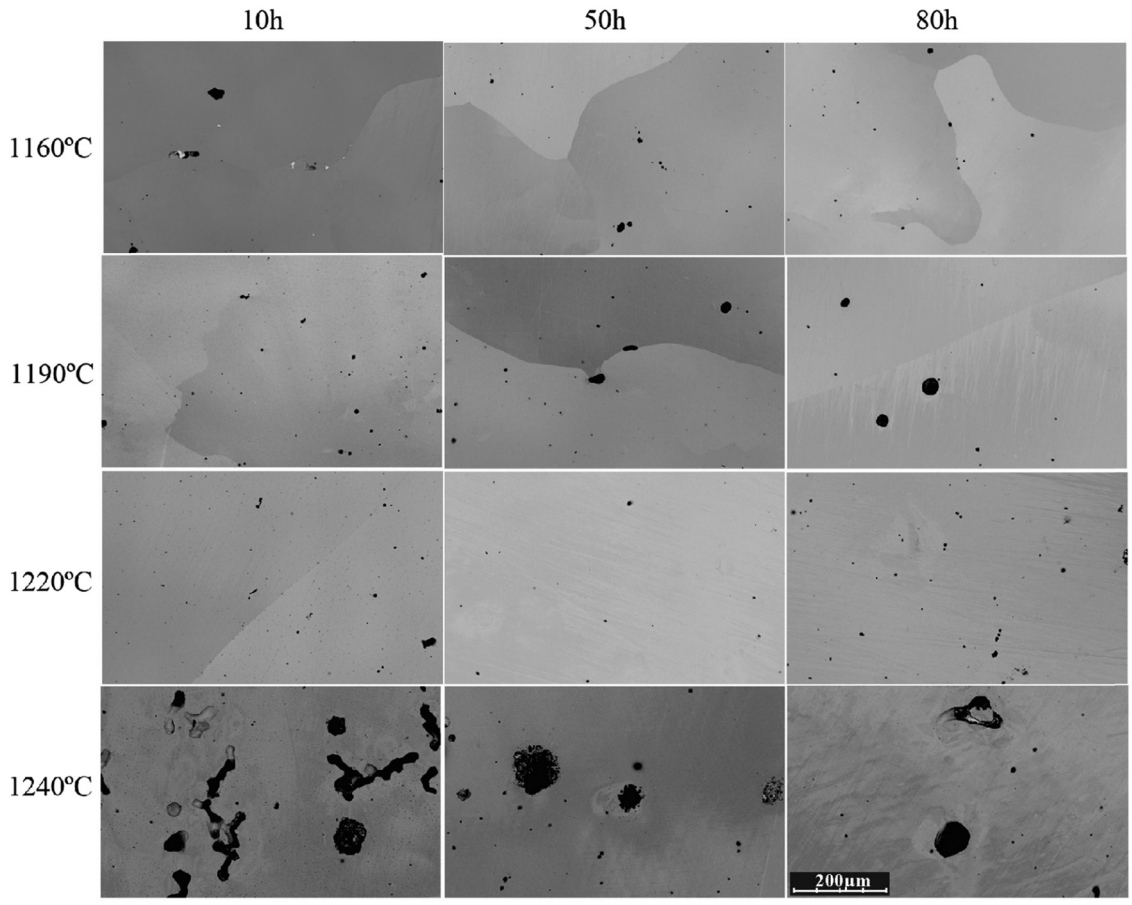

Figure 7: SEM morphology of samples from Disk I treated by a variety of homogenization schemes.

though blurred. Such a result means that this condition of homogenization has not completely dissolved the dendrites. In regard to grain size, it is found that not a complete grain is contained in the 15 mm × 15 mm surface of metallograph sample, indicating that the grain size has grown up to a level equivalent to 15 mm × 15 mm. In the literature, it is reported that the carbon content of René 65 is limited to a very low level in order to obtain an excellent fatigue property, and accordingly there are not enough carbides precipitated on grain boundaries to restrict the growth of grains [8,9]. As a result, significant growth of grains during homogenization is almost inevitable. Microstructures obtained by 1,160°C for 50 or 80 h exhibit similar features to that obtained by 1,160°C for 10 h, except that dendrites have been completely dissolved. Microstructure obtained by 1,190°C for 10 h is also similar to that of 1,160°C for 10 h, where eutectic phase has dissolved, grain boundaries are still visible, and dendrites are still distinguishable in some regions. When homogenization duration is prolonged to 50 h, dendrites are no longer distinguishable, and several small round pores about Ø 20 μm appear in matrix, which are left by quickly dissolving interdendritic regions. When it comes to 80 h, grain boundaries are turned from curved to straight, indicating that the grain size has further increased. In addition, bigger pores due to dissolving of interdendritic regions are found in matrix as well. Microstructure obtained by 1,220°C for 10 h exhibits neither visible eutectic phase nor dendrites, and grain boundaries have become straight like 1,190°C for 80 h. When duration is increased to 50 h, no visible grain boundary is found in the 15 mm × 15 mm sample surface, suggesting that the grain size has become even greater than a 15 mm × 15 mm area. When it comes to 80 h, microstructure is similar to that of 50 h, and no grain boundary is found in the metallograph sample. Microstructures obtained by 1,240°C for 10, 50, and 80 h exhibit many pores of diameter >100 μm in matrix, and no grain boundaries are found in those samples. Such a temperature is very close to the initial melting temperature of René 65, hence many interdendritic regions have been melted or quickly dissolved into matrix, leaving intensive pores.

As a result, it can be concluded that 1,240°C is a temperature too high for homogenization of René 65 because intensive pores generated may cause cracks in deformation. At other temperatures, microstructure analysis indicates that the grain size of René 65 grows up in a relatively fast rate during homogenization. In terms of avoiding overgrowth of grains and intensive pore generation, 1,160°C is an acceptable temperature for homogenization.

Figure 8 shows homogenized microstructures of samples from Disk II under SEM. In the group of 1,140°C, one may find that there still exist grey-colored blocks of γ–γ′ eutectic phase, which are shrinking with processing time, but not completely dissolved even when homogenized for 80 h. Processing time of 80 h is a considerably long duration in industrial practice, hence to homogenize René 65 at 1,140°C is not an optimized scheme, even for a small ingot with 95 μm SDAS. In contrast, 1,160°C is able to complete dissolve γ–γ′ eutectic phase. As shown in the image of 1,160°C for 10 h, eutectic phase has been eliminated, and grain boundaries are still visible, but dendrites are not distinguishable by black–white backscatter contrast due to intensive γ′ dispersion. Such intensity of γ′ dispersion is possibly relevant to the bigger size of blocks machined for homogenizing, which leads to slower cooling in the air, and eventually leads to an increase in size and more intensive dispersion of γ′ [33]. Apart from precipitated γ′, each microstructure of 1,160°C is very similar to the corresponding microstructure of 1,160°C in Figure 7.

Homogenized microstructure analysis of Disk I demonstrates that 1,190°C is the upper limit of homogenization for René 65 because pores due to phase dissolving start to appear given 50 or 80 h processing time and curved grain boundaries are turning straight given 80 h processing time. Homogenized microstructure analysis of Disk II demonstrates that 1,140°C is the lower limit of homogenization for René 65 because blocks of γ–γ′ eutectic phase still exist given 80 h processing time. Therefore, in respect of microstructure, 1,160°C is an acceptable temperature among these selected temperatures.

3.2.2 Residual segregation index evolution in homogenization

Apart from microstructure analysis, residual segregation index δ is an index generally used to characterize the result of homogenization of alloys, defined by:

$$\delta = \frac{C_{\max} - C_{\min}}{C_{0\max} - C_{0\min}},$$

where $C_{\max}$ and $C_{\min}$ represent the highest and lowest concentration of a given element after homogenization, respectively, and $C_{0\max}$ and $C_{0\min}$ represent the highest and lowest concentration of the element before homogenization, respectively. Theoretically, initial δ is equal to unity and complete homogenization means $\delta = 0$. In general industrial practice, homogenization is considered acceptable when δ is brought down below 0.2. The present study employs SEM and EDS to measure the value of each term in the formula, and the method of measurement is described as follows. Prior to homogenization, as dendrites are able to be clearly identified, 10 measuring regions are marked dendritically as well as inter-dendritically at 700 times magnification, respectively, summing up to 20 measuring regions. For a given element, the highest and lowest concentration measured in these

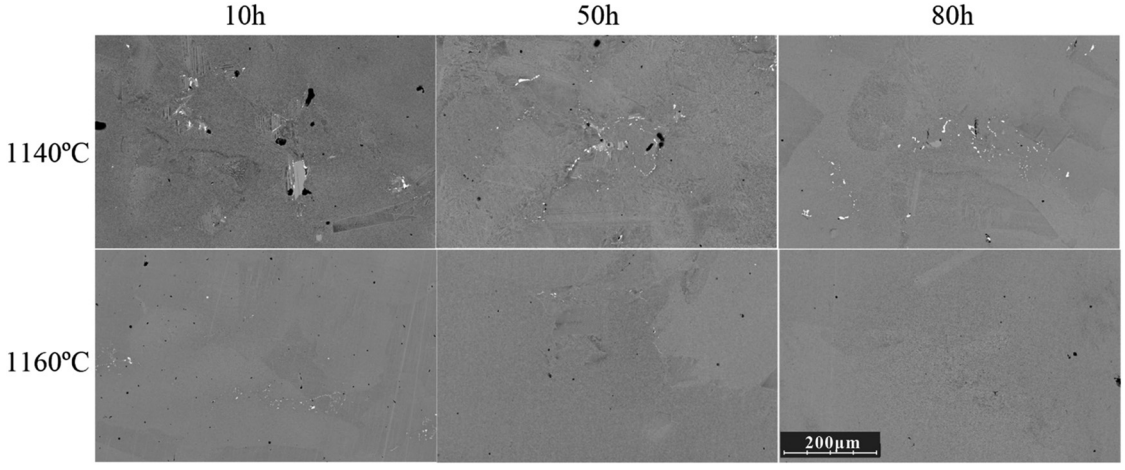

Figure 8: SEM morphology of samples from Disk II treated by a variety of homogenization schemes.

20 measuring regions is considered values for C_{0max} and C_{0min}, respectively. After homogenization, dendrites have been faded out, hence it is not applicable to exactly track elements at dendrites or interdendritic regions under SEM scope. Therefore, the present study applies the following method to measure element concentration. At 700 times magnification, 10 measuring regions are marked from top left to bottom right of the current SEM scope, where the size of each marked region accounts for about 1/10 of the current SEM scope, and the highest and lowest concentration measured among the 10 regions is considered C_{max} and C_{min} for the given element, respectively. Although it is not an accurate method to measure element concentration by using SEM regional marking, the results are still able to represent approximate concentration changes of a certain element in homogenizing process. Such a method entails less measurement time than electron probe microscope analysis, hence the present study employs this method to determine element concentrations in homogenized samples.

The trends in residual segregation index δ of the four critically segregated elements Ti, Nb, Mo, and W are shown in Figure 9. It is illustrated that values of δ are identically dropping fast within 10 h homogenizing time but the tendency is turning flat after 10 h. At 1,160 or 1,190°C, 10 h processing is able to bring down the residual segregation index δ of Ti, Nb, or Mo to 0.2 or less, whereas 80 h processing is able to bring down δ_W to about 0.3, still above 0.2. Hence, segregation of W is the most difficult to mitigate in René 65. At 1,220 or 1,240°C, 80 h homogenization is able to bring down δ_W to less than 0.2, but concomitant overgrowth of grains or generation of pores is inevitable, as shown in Figure 7.

Figure 10 illustrates residual segregation index of samples from Disk II. The image of 1,140°C shows that δ of each element varies in a very wide range along processing time, suggesting that segregation is barely mitigated. It is noticeable that some dots are even greater than unity. It is because measurement of δ of each element is based on maximum and minimum concentrations

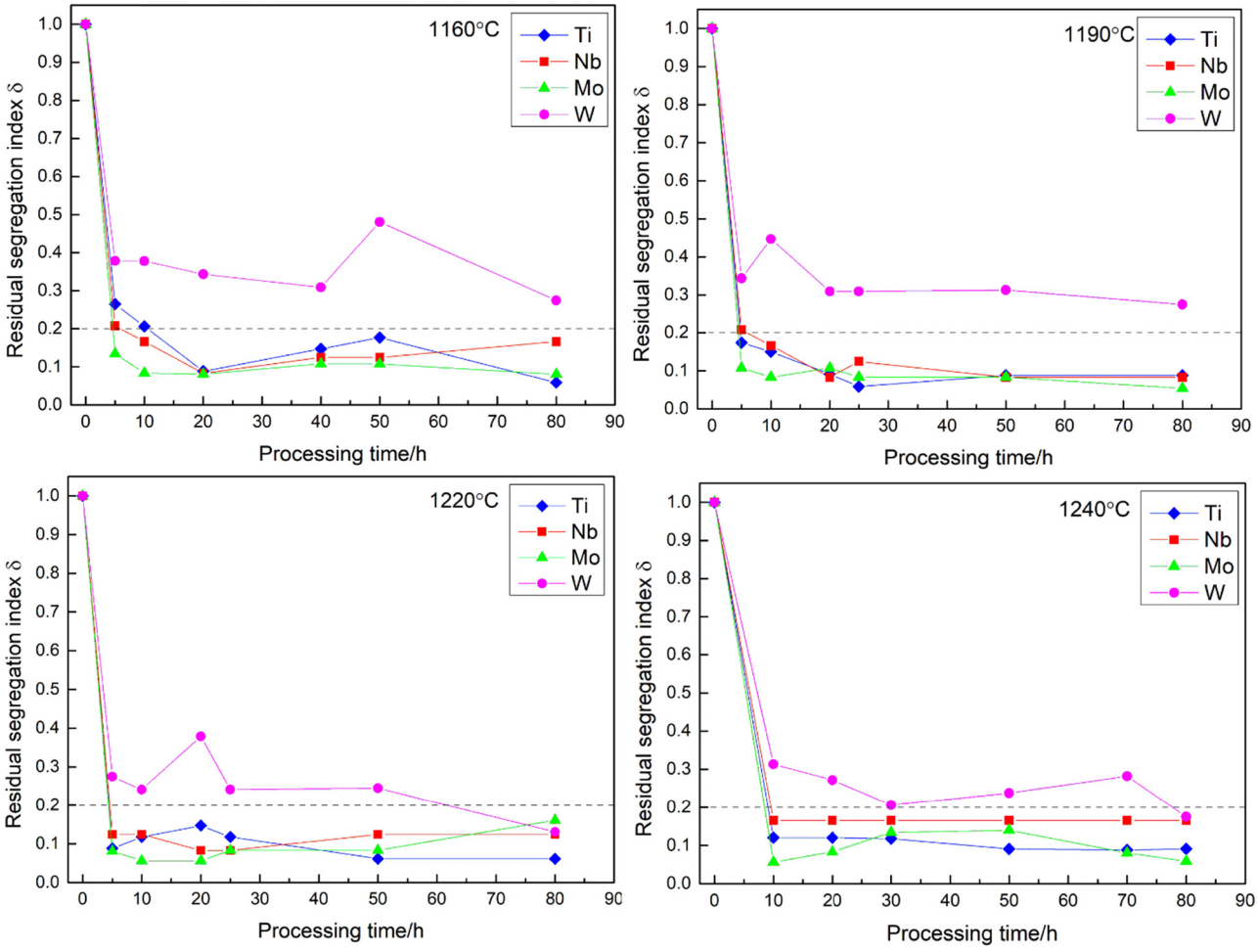

Figure 9: Residual segregation index evolution of samples from Disk I at a variety of homogenization temperatures.

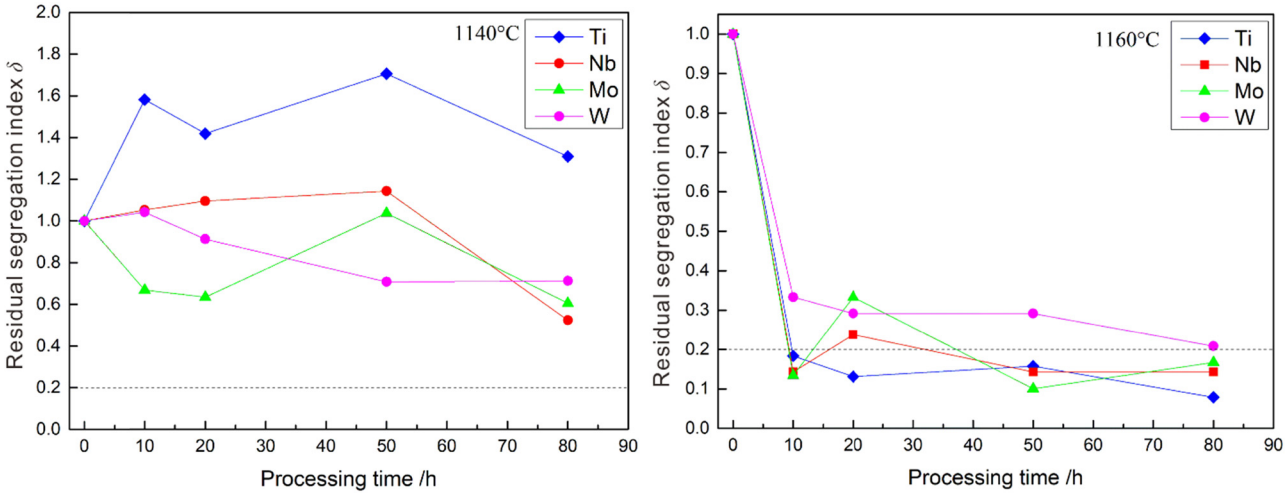

Figure 10: Residual segregation index evolution of samples from Disk II at a variety of homogenization temperatures.

in a certain microscope. If the processing temperature is set too low or the processing duration is not long enough, the gap between the maximum and minimum may be very significant, which leads to a greater calculated value of δ than unity. Such a result indicates that 1,140°C is a temperature too low for homogenization of René 65, even the sample from Disk II with a smaller SDAS cannot be homogenized. The image of 1,160°C illustrates similar trends to the image of 1,160°C in Figure 9. δ of Ti, Nb, or Mo has been brought down to 0.2 by 80 h processing, and δ of W is decreased to a level very close to 0.2. This is better than that obtained by 1,160°C for 80 h in Disk I since SDAS in Disk II is smaller.

The above microstructure analysis and residual segregation index evolution both confirm that 1,140°C is too low a temperature to homogenize René 65. However, for the other temperatures, evidence from these two aspects result in paradoxical conclusions. If microstructure with less defects and smaller grains is desired, segregation of W will be critical. On the contrary, if mitigated segregation of W is desired, more defects and growth of grain will be present in matrix. Hence, a comprehensive discussion is needed for a proper homogenization scheme.

3.3 Discussions for a proper homogenization scheme of René 65

From the aspect of microstructure, 1,160°C for 80 h is an acceptable scheme for Disk I of 115 μm SDAS, as γ–γ′ eutectic phase has been dissolved and growth of grains is acceptable. Nevertheless, residual segregation index at 1,160°C shows that 80 h processing is not able to decrease δ_W to industrially desired level 0.2 in Disk I. Hence, to make W further homogenized, a longer duration at 1,160°C is needed. Predictably, a longer homogenization processing time leads to further growth of grains, resulting in bad subsequential forge performance. In addition, a longer processing time brings issues of more energy consumption and a lower rate of production. To reduce cost, we can estimate how long duration of homogenization is needed to decrease δ_W in Disk I to 0.2 by using kinetics equation for dendrite diffusivity and data obtained in Disk II [24,26,27]. As shown in Figure 10, 1,160°C for 80 h is able to decrease δ_W in Disk II to 0.2 due to its smaller SDAS. The kinetics equation is expressed as:

$$C(x,t) = \bar{C} + \frac{1}{2}\Delta C \cos\left(\frac{2\pi x}{L}\right)\exp\left(-\frac{4\pi^2}{L^2}Dt\right), \quad (1)$$

which assumes concentration of a given element distribution along dendrites and interdendritic regions as a cosine function, where $C(x,t)$ denotes the concentration of the element at the location of x and at the moment of t in homogenization, as shown in Figure 11. In equation (1), $\bar{C}$ denotes the average concentration of a given element, ΔC denotes the gap between maximum and minimum concentration when $t = 0$, L denotes SDAS, and D the interdiffusion coefficient of a certain element. By substituting $x = 0$ and $x = L/2$ into equation (1), one may obtain maximum and minimum concentrations of given element at any moment t of homogenization, and residual segregation index δ can be computed by

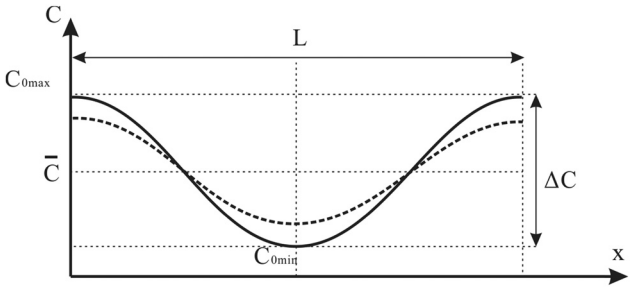

Figure 11: Schematic diagram of cosine distribution of element concentration.

$$\delta = \frac{C(0,t) - C\left(\frac{1}{2}L, t\right)}{C_{0\max} - C_{0\min}} = \exp\left(-\frac{4\pi^2}{L^2}Dt\right), \tag{2}$$

where D is calculated by:

$$D = D_0 \exp\left(-\frac{Q}{RT}\right), \tag{3}$$

where T denotes the temperature, R the ideal gas constant, D_0 the diffusivity, and Q the activation energy of diffusion. D_0 and Q are both impacted by the medium in which atoms of the element are diffusing, namely, the matrix, hence we cannot directly apply values obtained in X-Ni binary alloys into René 65. However, we can assume that D_0 and Q in Disk I are equivalent to those in Disk II due to close compositions of the two. Accordingly, for a certain element, given the same level of residual segregation index δ, we have viz.

$$\delta_{\mathrm{I}} = \delta_{\mathrm{II}}, \tag{4}$$

$$-\frac{4\pi^2}{L_I^2}D_I t_I = -\frac{4\pi^2}{L_{\mathrm{II}}^2}D_{\mathrm{II}} t_{\mathrm{II}}. \tag{5}$$

As D_{I} is assumed to be equivalent to D_{II}, we have

$$t_{\mathrm{I}} = \left(\frac{L_{\mathrm{I}}}{L_{\mathrm{II}}}\right)^2 t_{\mathrm{II}}. \tag{6}$$

Given $L_{\mathrm{I}} = 115$ μm, $L_{\mathrm{II}} = 90$ μm as measured in Figure 3, and time needed to decrease δ_{W} to 0.2 in Disk II $t_{\mathrm{II}} = 80$ h, equation (6) yields $t_{\mathrm{I}} = 131$ h. It means that 131 h is needed to decrease δ_{W} to the equivalent level 0.2 in Disk I, which is a duration far beyond normal homogenization time in industrial practice.

Previous researchers studied the impact of extent of homogenization on deformation behavior and revealed that post-homogenization residual dendrites are able to provide nucleation sites for recrystallization in deformation [34]. From this perspective, complete homogenization of as-cast microstructure may not be the optimized choice, and the determination of homogenization scheme should take deformation performance into consideration. As a result, we use samples from Disk II to conduct thermal compression experiment for the purpose of understanding the impact of homogenization on deformation behavior. Compression is conducted at a common billet conversion condition for Ni-base superalloy: 1,150°C, 0.1 s^{-1} strain rate, and 30% engineering strain, and the results are shown in Figure 12.

Samples after compression shown in Figure 12 exhibit no visible cracks, hence curves in Figure 12 represent true flow stress due to internal microstructure evolution in deformation. It is found that flow stress of 50 h homogenization is the lowest among the four, while 80 h is the highest. Flow stresses of 10 and 20 h are almost in a same level between 50 and 80 h. Peak stress along homogenization time shows a trend of first decreasing

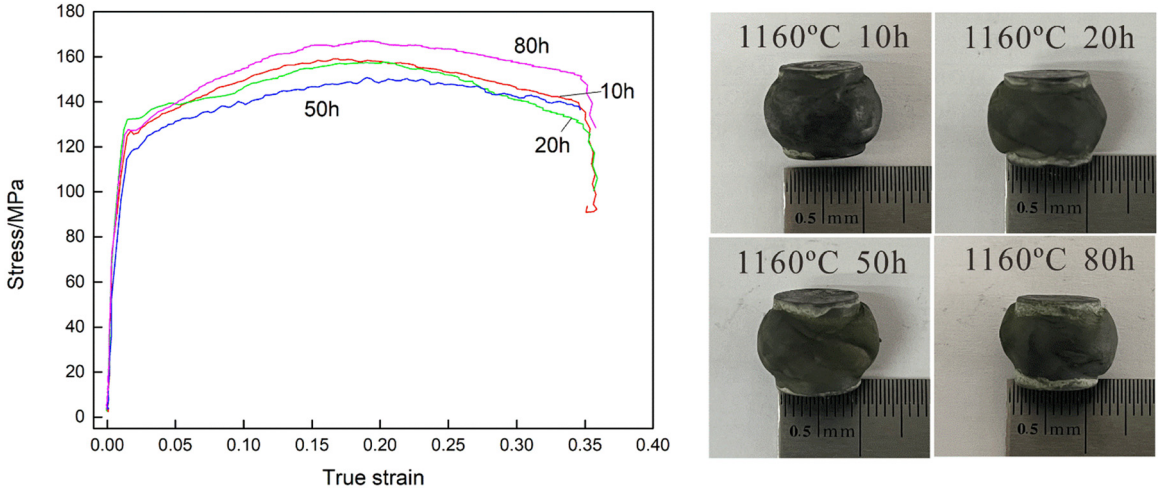

Figure 12: Flow stress curves of samples from Disk II, at 1,150°C, 0.1 s^{-1}, 30%.

and then increasing. This result suggests that microstructure of Disk II obtained by 1,160°C for 50 h is more suitable for deformation than the other processing durations in respect of deformation performance. It is notable that Figure 10 shows that 1,160°C for 50 h is merely able to decrease δ_W to around 0.3, which means that to decrease δ of each element below 0.2 is not a necessary precondition to create appropriate microstructure for deformation. On the contrary, decreasing δ of every element to 0.2 or below results in an increase in flow stress, which is not preferred by the process of deformation. Ideally, such a comparison of flow stresses of samples that have undergone different homogenization schemes should also be conducted using samples from Disk I, but Disk I is cut from the top end of a Ø 450 mm ingot, where defects are more intensive than Disk II. Due to the existence of such defects, cracking occurs in samples in thermal compression, and thus no credible flow stress curve can be obtained. Nevertheless, we may still estimate the appropriate homogenization duration of Disk I by equation (6). At 1,160°C, given L_I = 115 μm, L_{II} = 90 μm, and the appropriate duration in Disk II t_{II} = 50 h, equation (6) yields t_I = 82 h. It means that, in Disk I at 1,160°C, it takes 82 h for segregation of elements to get mitigated to the extent of that in Disk II for 50 h, which is a duration able to create suitable microstructure for deformation. Microstructure and residual segregation index obtained by 1,160°C for 80 h in Disk I can be used as a verification of the estimation, with only 2 h deviation. It is found that microstructure of 1,160°C for 80 h in Figure 7 is very similar to that of 1,160°C for 50 h in Figure 8, including γ–γ′ eutectic phase dissolved, grain boundaries clearly visible and curved, no dendrites visible by black–white contrast under SEM. Likewise, residual segregation index δ of each element at 1,160°C for 80 h in Figure 9 is also on an equivalent level of that at 1,160°C for 50 h in Figure 10, namely δ_{Ti}, δ_{Nb}, and δ_{Mo} in the range of 0.1–0.2, while δ_W around 0.3. Hence, we can conclude that for a Ø 450 mm René 65 ingot, 1,160°C for 82 h is an applicable homogenization scheme, by which γ–γ′ eutectic phase and dendrites can be dissolved, grain boundaries remain curved, δ_{Ti}, δ_{Nb}, and δ_{Mo} are decreased to below 0.2, δ_W is decreased to around 0.3, and flow stress is estimated in a low level.

4 Conclusions

In this article, we use René 65 samples from a Ø 450 mm ESR ingot and a Ø 250 mm pilot VAR ingot to investigate as-cast microstructure and homogenization schemes of the alloy. The following points are concluded.

(1) In as-cast René 65, main precipitated phases include γ–γ′ eutectic phase, irregular borides–carbides, and dispersed polygonal TiN. Eutectic phase is the key phase that needs to be dissolved in homogenization due to its hardness and brittleness.
(2) In as-cast René 65, critically segregated elements include Ti, Nb, Mo, and W, where Ti, Nb, and Mo concentrate at interdendritic regions while W concentrates at dendrites.
(3) From the aspect of microstructure, the upper limit of temperature for homogenization of René 65 is 1,190°C because pores due to phase dissolving start to appear given 50 or 80 h processing and curved grain boundaries are turning straight given 80 h processing. The lower limit is 1,140°C because blocks of γ–γ′ eutectic phase still exist given 80 h processing. Hence, 1,160°C is the acceptable temperature for homogenization of René 65 among the temperatures in the present study.
(4) Residual segregation index analysis shows that segregation of W is the most difficult to eliminate in René 65. In Disk I, with SDAS = 115 μm, 1,160 h for 80 h is able to decrease δ_{Ti}, δ_{Nb}, and δ_{Mo} to less than 0.2 and δ_W to 0.3, while in Disk II, with SDAS = 90 μm, the same condition is able to decrease δ_{Ti}, δ_{Nb}, and δ_{Mo} to less than 0.2 and δ_W to 0.2.
(5) Thermal compression experiment by using homogenized samples from Disk II shows that 1,160°C for 50 h provides the lowest flow stress among the four durations. It is estimated according to kinetics equation for dendrites diffusion that it takes about 1,160°C for 82 h to obtain the equivalent effect in Disk I. Such a result is verified by similarity of microstructure as well as equivalence of residual segregation index between Disk I of 1,160°C for 80 h and Disk II of 1,160°C for 50 h.

Acknowledgments: The authors would like to thank Material Analysis and Characterizing Center, Chengdu Institute of Advanced Metallic Material Technology and Industry Co. Ltd.

Funding information: Author states no funding involved.

Author contributions: Dr. Lang Shui contributed in conceptualization, methodology, literature review, writing, manuscript review and project administration. Mr. Jianhui Fu contributed in literature review, experimental

operation, sample characterizing, and manuscript review.

Conflict of interest: The authors state no conflict of interest.

References

[1] Wlodek, S. T., M. Kelly, and D. A. Alden. The structure of René 88 DT. *Proceedings of Superalloys 1996, September 22–26, 1996, Champion*, TMS, Pennsylvania, USA, 1996, pp. 129–136.

[2] Krueger, D. D., R. D. Kissinger, R. G. Menzies, and C. Wukusick. Fatigue crack growth resistant nickel-base article and alloy and method for making. U.S. Patent No. 4957567, 1990.

[3] Babu, S. S., M. K. Miller, J. M. Vitek, and S. A. David. Characterization of the microstructure evolution in a nickel base superalloy during continuous cooling conditions. *Acta Materilia*, Vol. 49, No. 20, 2001, pp. 4149–4160.

[4] Mao, J., K. Chang, W. Yang, D. U. Furrer, K. Ray, and S. P. Vaze. Cooling precipitation and strengthening study in powder metallurgy superalloy René 88 DT. *Materials Science and Engineering A*, Vol. 332, No. 1–2, 2002, pp. 318–329.

[5] Hwang, J. Y., R. Banerjee, J. Tiley, J. R. Srinivasan, G. B. Viswanathan, and H. L. Fraser. Nanoscale characterization of elemental partitioning between gamma and gamma prime phases in René 88 DT nickel-base superalloy. *Metallurgical and Materials Transactions A*, Vol. 40, No. 1, 2009, pp. 24–35.

[6] Singh, A. R. P., S. Nag, J. Y. Hwang, G. B. Viswanathan, J. Tiley, R. Srinivasan, et al. Influence of cooling rate on the development of multiple generations of γ′ precipitates in a commercial nickel base superalloy. *Materials Characterization*, Vol. 62, No. 9, 2011, pp. 878–886.

[7] Singh, A. R. P., S. Nag, S. Chattopadhyay, Y. Ren, and R. Banerjee. Mechanism related to different generations of γ′ precipitation during continuous cooling of a nickel base superalloy. *Acta Materilia*, Vol. 61, No. 1, 2013, pp. 280–293.

[8] Heaney, J. A., M. L. Lasonde, A. M. Powell, B. J. Bond, and C. M. O'Brien. Development of a new cast and wrought alloy (René 65) for high temperature disk applications. *Proceedings of the 8th International Symposium on Superalloy 718 and Derivatives*, TMS, Pittsburgh, USA, September 28–October 1, 2014, pp. 67–77.

[9] Bond, B. J., C. M. O'Brien, J. L. Russell, J. A. Heaney, and M. L. Lasonde. René 65 billet material for forged turbine components. *Proceedings of the 8th International Symposium on Superalloy 718 and Derivatives*, TMS, Pittsburgh, USA, September 28–October 1, 2014, pp. 107–118.

[10] Minisandram, R. S., L. A. Jackman, J. L. Russell, M. L. Lasonde, J. A. Heaney, and A. M. Powell. Recrystallization response during thermo-mechanical processing of alloy René 65 billet. *Proceedings of the 8th International Symposium on Superalloy 718 and Derivatives*, TMS, Pittsburgh, USA, September 28–October 1, 2014, pp. 95–105.

[11] Laurence, A., J. Cormier, P. Villechaise, T. Billot, J. M. Franchet, F. Pettinari-Sturmel, et al. Impact of the solution cooling rate and of thermal aging on the creep properties of the new cast & wrought René 65 Ni-based superalloy. *Proceedings of the 8th International Symposium on Superalloy 718 and Derivatives*, TMS, Pittsburgh, USA, September 28–October 1, 2014, pp. 333–348

[12] Olufayo, O. A., H. Che, V. Songmene, C. Katsari, and S. Yue. Machinability of Rene 65 superalloy. *Materials*, Vol. 12, No. 12, 2019, id. 2034.

[13] Gourdin, S., J. Cormier, G. Henaff, Y. Nadot, F. Hamon, and S. Pierret. Assessment of specific contribution of residual stress generated near surface anomalies in the high temperature fatigue life of a René 65 superalloy. *Fatigue & Fracture of Engineering Materials & Structures*, Vol. 40, No. 1, 2017, pp. 69–80.

[14] Wojcik, T., M. Rath, and E. Kozeschnik. Characterisation of secondary phases in Ni-base superalloy René 65. *Materials Science and Technology*, Vol. 34, No. 13, 2018, pp. 1558–1564.

[15] Charpagne, M. A., P. Vennegues, T. Billot, J. M. Franchet, and N. Bozzolo. Evidence of multimicrometric coherent γ′ precipitates in a hot-forged γ–γ′ nickel-based superalloy. *Journal of Microscopy*, Vol. 263, No. 1, 2016, pp. 106–112.

[16] Zhang, B., G. Zhao, W. Zhang, G. Xu, and H. Qin. Deformation mechanisms and microstructural evolution of γ + γ′ aggregates generated during thermomechanical processing of nickel-base superalloys. *Proceedings of the 13th International Symposium on Superalloys*, TMS, Seven Springs, Pennsylvania, USA, September 11–15, 2016, pp. 487–496.

[17] Zhao, G., S. Huang, B. Zhang, G. Xu, H. Qin, and W. Zhang. Microstructure control and mechanical properties of the newest nickel-based wrought superalloy GH4065A. *Journal of Iron and Steel Research*, Vol. 27, No. 2, 2015, pp. 37–44.

[18] Huang, S., B. Zhang, Q. Tian, G. Zhao, G. Xu, and H. Qin. Isothermal and static oxidation behavior of superalloy GH4065A. *Journal of Iron and Steel Research*, Vol. 28, No. 7, 2016, pp. 55–60.

[19] Du, J., G. Zhao, and Q. Deng. Development of wrought superalloy in China. *Journal of Aeronautical Materials*, Vol. 36, No. 3, 2016, pp. 27–39.

[20] Wang, Z., S. Huang, B. Zhang, L. Wang, and G. Zhao. Study on freckle of a high-alloyed GH4065 nickel base wrought superalloy. *Acta Metallurgica Sinica*, Vol. 55, No. 3, 2019, pp. 417–426.

[21] Liu, Q., S. Huang, J. Liu, C. Zhang, R. Fang, and H. Pei. Progress and application of high temperature structure materials on aero-engine. *Gas Turbine Experiment and Research*, Vol. 27, No. 4, 2014, pp. 51–56.

[22] Zhang, B., G. Zhao, W. Zhang, S. Huang, and S. Chen. Investigation of high performance disc alloy GH4065 and associated advanced processing techniques. *Acta Metallurgica Sinica*, Vol. 51, No. 10, 2015, pp. 1227–1234.

[23] Zhang, B., S. Huang, and W. Zhang. Recent development of nickel-based disc alloys and corresponding cast-wrought processing techniques. *Acta Metallurgica Sinica*, Vol. 55, No. 9, 2019, pp. 1095–1114.

[24] Purdy, G. R. and J. S. Kirkaldy. Homogenization by diffusion. *Metallurgical Transactions*, Vol. 2, No. 2, 1971, pp. 371–378.

[25] Böttger, B., U. Grafe, and D. Ma. Prediction and measurement of microsegregation and microstructural evolution of directionally solidified superalloys. *Proceedings of Superalloys*

2000, the 9th International Symposium on Superalloys, TMS, Champion, Pennsylvania, USA, September 17–21, 2000, pp. 313–322.

[26] Karunaratne, M. S. A., D. C. Cox, P. Carter, and R. C. Reed. Modelling of the microsegregation in CMSX-4 superalloy and its homogenisation during heat treatment. *Proceedings of Superalloys 2000, the 9th International Symposium on Superalloy*s, TMS, Champion, Pennsylvania, USA, September 17–21, 2000, pp. 263–272.

[27] Semiatin, S. L., R. C. Kramb, R. E. Turner, F. Zhang, and M. M. Antony. Analysis of the homogenization of a nickel-base superalloy. *Scripta Materialia*, Vol. 51, No. 6, 2004, pp. 491–495.

[28] Reed, R. C., and C. M. F. Rae. *Physical metallurgy* (*fifth edition*), *chapter 22 physical metallurgy of the nickel-based superalloys*, Elsevier, Amsterdam, 2014.

[29] Garosshen, T. J., T. D. Tillman, and G. P. McCarthy. Effects of B, C, and Zr on the structure and properties of a P/M nickel base superalloy. *Metallurgical Transactions A*, Vol. 18, No. 1, 1987, pp. 69–77.

[30] Chen, W., M. Chaturvedi, N. Richards, and G. Mcmahon. Grain boundary segregation of boron in Inconel 718. *Metallurgical Transactions A*, Vol. 29, No. 7, 1998, pp. 1947–1954.

[31] Zhao, G., L. Yu, G. Yang, W. Zhang, and W. Sun. The role of boron in modifying the solidification and microstructure of nickel-base alloy U720Li. *Journal of Alloys and Compounds*, Vol. 686, 2016, pp. 194–203.

[32] Zhou, P. J., J. J. Yu, X. F. Sun, H. R. Guan, and Z. Q. Hu. The role of boron on a conventional nickel-based superalloy. *Materials Science & Engineering A*, Vol. 491, No. 1–2, 2008, pp. 159–163.

[33] Zhao, G., G. Yang, F. Liu, X. Xin, and W. R. Sun. Transformation mechanism of γ + γ′ and the effect of cooling rate on the final solidification of U720Li alloy. *Acta Metallurgia Sinica*, Vol. 30, No. 9, 2017, id. 894.

[34] Dong, J., L. Li, H. Li, M. Zhang, and Z. Yao. Effect of extent of homogenization on the hot deformation recrystallization of superalloy ingot in cogging process. *Acta Metallurgia Sinica*, Vol. 5110, 2015, pp. 1207–1218.